

# Polarization oscillating beams constructed by copropagating optical frozen waves

PENG LI,<sup>1,3</sup> DONGJING WU,<sup>1</sup> YI ZHANG,<sup>1</sup> SHENG LIU,<sup>1</sup> YU LI,<sup>1,2</sup> SHUXIA QI,<sup>1</sup> AND JIANLIN ZHAO<sup>1,4</sup>

<sup>1</sup>MOE Key Laboratory of Material Physics and Chemistry under Extraordinary Conditions, and Shaanxi Key Laboratory of Optical Information Technology, School of Science, Northwestern Polytechnical University, Xi'an 710129, China

<sup>2</sup>Department of Public Education, Northwestern Polytechnical University Ming De College, Xi'an 710124, China

<sup>3</sup>e-mail: pengli@nwpu.edu.cn

<sup>4</sup>e-mail: jlzhao@nwpu.edu.cn

Received 21 March 2018; revised 4 May 2018; accepted 24 May 2018; posted 24 May 2018 (Doc. ID 326558); published 27 June 2018

**Polarization oscillating beams, namely, polarization standing waves, commonly formed by a pair of coherent counterpropagating light waves with orthogonal polarizations, oscillate their states of polarization periodically within a wavelength interval, offering conceptual and practical interests in light-matter interactions such as the nonreciprocal magnetoelectric effect, and impressive applications in optical imaging, sensing, and chirality detection. Here, we propose a new class of polarization oscillating beams that longitudinally vary states of polarization with spatial intervals within centimeters via the superposition of two copropagating optical frozen waves with preshaped longitudinal intensity profiles and transverse phase structures. The flexibility and manipulability are demonstrated by creating several polarization oscillating beams with different polarization structures. This work paves a new way to manipulate other waves and may be useful for applications of optical standing waves in optical manipulation, light guiding of atoms, polarization-sensitive sensing, etc. © 2018 Chinese Laser Press**

**OCIS codes:** (260.5430) Polarization; (260.6042) Singular optics; (140.3300) Laser beam shaping.

<https://doi.org/10.1364/PRJ.6.000756>

## 1. INTRODUCTION

The standing wave, manifesting itself as a stationary wave that has static peak location and oscillating energy, has been widely observed in free space, media, resonators, and so on. As a canonical physical phenomenon, it can arise in all kinds of waves, including mechanical waves, sound waves, and light waves, etc. In the light-wave regime, more particularly, the standing wave formed by a pair of counterpropagating constituent waves with orthogonal polarizations, namely, the polarization standing wave, periodically varies the state of polarization (SoP) along the propagation direction [1], exhibiting natural polarization oscillation features. Hence, such beams are also named as polarization oscillating waves and have exhibited heuristic interests in scientific and application realms [2–11]. Remarkably, polarization oscillating waves have been employed to produce nonreciprocal magnetoelectric effects [3], enhanced light-matter interaction [2,4], nontrivial optical force [5,6], nonlinear optical phenomena [7,8], and further, have been introduced to facilitate the applications in chirality detection [9], sensing [10], etc.

As a common feature of the interference of two counterpropagating coherent waves, the polarization oscillating wave changes the transverse SoP periodically in an interval of a wavelength; that is, its longitudinal period identically equals the

wavelength. Recently, a new class of optical waves with variant SoP along the propagation axis and tunable period has been explored by steering two copropagating waves [11], exhibiting physical prospects involving light-matter interaction and application potential in optical manipulation and encryption. For instance, Cardano *et al.* generated Poincaré beams that rotate their transverse SoPs by using spiral wave plates, relying on the  $z$ -dependent Gouy phase difference between Laguerre–Gauss (LG) modes that compose Poincaré beams [12]. Moreno and Fu separately reported vector Bessel beams that periodically change transverse SoPs upon beam propagation [13–15]. Further, we constructed high-order vector Bessel beams with hybrid SoPs by engineering the Pancharatnam–Berry phases of constituent Bessel beams and demonstrated the self-healing feature of their three-dimensionally structured SoPs [16]. It should be noted, however, these vector Bessel beams possessing  $z$ -dependent SoPs also present quasi-Gauss intensity profiles along the  $z$  axis. Such unadjustable intensity profiles may well be a restrictive factor in practical applications.

In this paper, by quoting the stationary property of frozen waves [17–19], we propose a general principle for constructing polarization oscillating beams based on the axial superposition of two copropagating optical frozen waves with preshaped longitudinal intensity profiles and transverse phase structures.

Such fields have uniform intensities, but periodically oscillating SoPs in centimeter intervals along the propagating direction. Experimentally, we construct several polarization oscillating beams with zeroth- and higher-order SoPs by employing a  $4f$  polarization conversion system, indicating that this method is flexible and accurate for manipulation of the longitudinal oscillation of an SoP.

## 2. EXPERIMENTAL SETUP

Figure 1 schematically shows our construction principle of a polarization oscillating beam. It is well known that the SoP of a light wave can be intuitively depicted with a point on the Poincaré sphere, of which the location is dependent on the amplitude ratio and phase difference of two orthogonal states constructing the Poincaré sphere. This means that steering the complex amplitudes of two constituent waves enables the control of an SoP for an arbitrary optical field. With this principle, we consider the frozen waves that have arbitrarily controlled longitudinal intensity profiles as constituent beams.

A frozen wave, originally used to describe the beam keeping its shape in an absorbing medium, has been introduced to characterize the nondiffractive beam with a static intensity envelope, that is, the beam with intensity envelope velocity of  $v = 0$  [17], exhibiting a static property similar to a traditional standing wave. Generally, such beams are created from the superposition of copropagating Bessel beams with equal frequency but different transverse and longitudinal wavenumbers, exhibiting arbitrary  $z$ -dependent intensity profiles in defined propagation distances [17–19]. Moreover, as a new nondiffractive solution of a wave equation, the stable phase structure of a frozen wave also manifests itself as a desired candidate for steering the  $z$ -dependent SoP.

Supposing that a frozen wave is composed by  $2N + 1$  equal frequency Bessel beams of order  $l$ , its electric field thus can be defined by [17]

$$F(\rho, \phi, z, l) = e^{-i\omega t} \sum_{j=-N}^N A_j J_l(k_{\rho j} \rho) e^{ik_{zj} z} e^{il\phi}, \quad (1)$$

where  $k_{\rho j}^2 = \omega^2/c^2 - k_{zj}^2$  with  $k_{zj} = Q + 2\pi j/L$  and  $Q = (\omega^2/c^2 - 2.4^2/\rho_0^2)^{1/2}$  is the initial parameter determining the spot radius  $\rho_0$  of the Bessel beam,  $L$  is the finite distance maintaining a predefined longitudinal intensity profile,  $A_j$  is the weighting factor for the Bessel beam, and  $j$  is an integer.

In Fig. 1(a), we schematically present a zeroth-order frozen wave with a rectangular profile and a first-order frozen wave with a sinusoidal profile, respectively. Here, the intensity distribution is denoted as  $|F(\rho, z, l)|^2$ . The dashed lines denote where the intensity lines come from. These frozen waves both obviously present the desired longitudinal intensity profiles. It is noteworthy that, as a special solution of resonance, the sinusoidal function provides stability and smoothness for the longitudinal modulation. On the other hand, it is notable that the longitudinal intensity of a standing wave also presents a sinusoidal profile. Accordingly, we take the scenario that frozen waves have sinusoidal profiles as an example in the following content.

Figure 1(b) illustrates the construction of a polarization oscillating beam based on two sinusoidal frozen waves with opposite spin states and complementary intensity profiles. The red and blue lines depict the real parts [denoted as  $\text{Re}(F_1)$  and  $\text{Re}(F_2)$ ] of two frozen waves, respectively. As shown, two sinusoidal profiles have a  $\pi/2$  phase shift, that is, the longitudinal intensity profiles of two frozen waves can be, respectively, denoted by sinusoidal and cosine functions, which ensures the constructed polarization oscillating beam keeps a uniform intensity profile, namely,  $|F_1(\rho, \phi, z, l)|^2 + |F_2(\rho, \phi, z, l)|^2 \propto |J_l(\rho, \phi)|^2$ , where  $J_l(\rho, \phi)$  is an  $l$ th order Bessel function independent of  $z$ . Supposing that these two constituent frozen waves have a constant phase difference of  $\varphi_0 = -\pi/2$ , and expanding this issue into a more general case, these two frozen waves separately carry orbital angular momenta (OAMs) of  $m\hbar$  and  $n\hbar$ . Consequently, the SoP of the resultant polarization oscillating beam will periodically change along the meridian  $|\mathbf{R}_m\rangle \rightarrow |\mathbf{A}_{m,n}\rangle \rightarrow |\mathbf{L}_n\rangle \rightarrow |\mathbf{D}_{m,n}\rangle \rightarrow |\mathbf{R}_m\rangle$  on the hybrid Poincaré sphere [20], as the red curve shows in Fig. 1(c), where  $|\mathbf{R}_m\rangle$  and  $|\mathbf{L}_n\rangle$  depict the right- and left-handed circular polarizations with  $m$ th and  $n$ th order vortex phases, and  $|\mathbf{A}_{m,n}\rangle$  and  $|\mathbf{D}_{m,n}\rangle$  depict the diagonal and antidiagonal hybrid states, respectively. Note that the hybrid Poincaré spheres degenerate into a high-order Poincaré sphere when  $m = -n$  [21], but a canonical Poincaré sphere when  $m = n = 0$ .

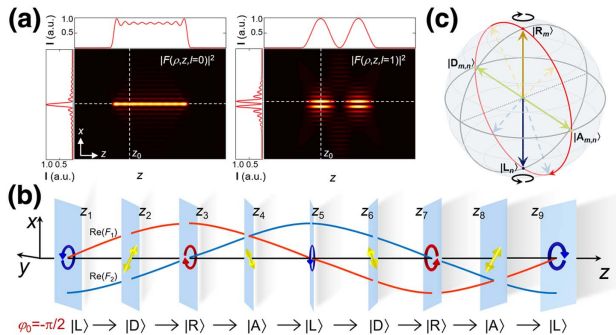


**Fig. 1.** Illustration of constructing polarization oscillating beams. (a) Zeroth- and first-order frozen waves that have rectangular and sinusoidal intensity profiles, respectively. The dashed lines denote where the intensity lines come from. (b) Evolution of transverse SoP of a polarization oscillating beam constructed from two sinusoidal frozen waves with opposite spin states and initial phase difference  $\varphi_0 = -\pi/2$ . The red and blue lines schematically depict the real parts of two electric fields. (c) Hybrid Poincaré sphere and the SoP conversion trajectory corresponding to the evolution in (b).

## 3. EXPERIMENTAL RESULTS AND DISCUSSION

According to this principle, we experimentally construct polarization oscillating beams by using the setup schematically shown in Fig. 2 [22–24]. The collimated and expanded laser beam (from an  $\text{Ar}^{3+}$  laser with a wavelength of  $\lambda = 514.5$  nm and waist radius about  $\omega_0 = 5$  mm) inputs into a beam splitter (BS). The transmitted part from the BS is absorbed by a beam terminal, and the other part is reflected onto the spatial light modulator (SLM) (Holoeye, Pluto) and encoded with pupil phases, and then passes through the BS and a lens. A filter

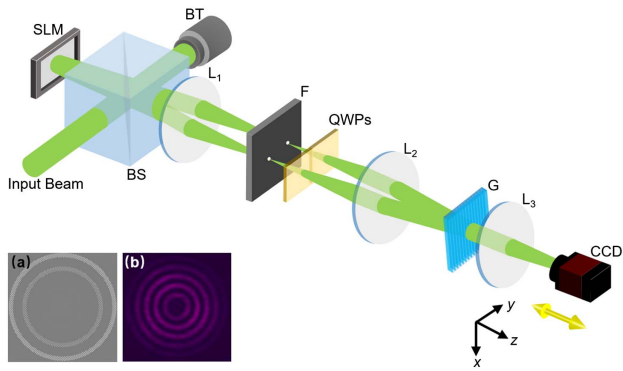


**Fig. 2.** Experiment setup for constructing polarization oscillating beams. SLM, spatial light modulator; BS, beam splitter; BT, beam terminal; L, lens; F, filter; QWP, quarter-wave plate; G, grating; CCD, charge-coupled device. Insets: (a) computer-generated hologram encoded on SLM; (b) intensity pattern of a first-order frozen wave at a certain location.

is used to choose the first-order diffractive beams. Two first orders then occur in opposite polarization conversion after two orthogonal quarter-wave plates and become circularly polarized beams. Two constituent beams passing through another lens then are axially synthesized by a Ronchi grating. Here the Ronchi grating and SLM are conjunctive in the  $4f$  system composed by lenses  $L_1$  and  $L_2$  with a focal length of 40 cm. This means that the output plane with grating is actually a spectrum plane of Bessel beams, so another focusing lens ( $L_3$ ) is employed to implement the Fourier transform. The resultant fields are observed by a CCD camera in linear motion.

The pupil phase encoded on the SLM actually is a computer-generated hologram for predefining the longitudinal intensity profiles of orthogonally polarized frozen waves. In practice, we define the sinusoidal profile in a finite distance of  $L = 44$  cm. The predefined amplitude profiles of two frozen waves are  $F_R(z, m = 0) = \sin(\pi z/\Lambda)$  and  $F_L(z, n = 0) = \cos(\pi z/\Lambda)$ , respectively. Here,  $\Lambda$  is the constant longitudinal period of intensity profile. The initial parameters are  $Q = 0.999992k$ , with  $k$  the wavenumber,  $N = 6$ , and  $\Lambda = 9.6$  cm. For such a case, the coefficients  $A_j$  are calculated according to [18]

$$A_j = \frac{1}{L} \int_0^L F(z, l) e^{-2\pi j z/L} dz. \quad (2)$$

It is well known that Bessel beams can be created from the Fourier transform of concentric rings [25]. This means that the pupil phase encoded on the SLM actually is employed to modulate the spectrum of each Bessel beam, namely, the concentric rings. Therefore, the pupil phase is a superposition of concentric rings modulated by coefficients  $A_j$  and spiral phases  $\exp(il\phi)$ . The insets in Fig. 2 display the computer-generated hologram and the corresponding intensity pattern of one frozen wave in a certain plane.

In compliance with this method, we first construct a fundamental polarization oscillating beam, namely, the zeroth-order Bessel field. For such a case, two orthogonal basic states

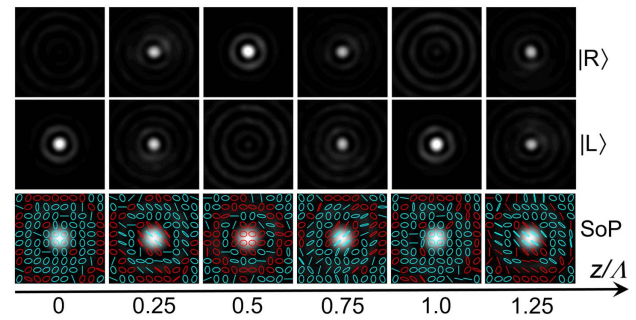


**Fig. 3.** Intensities of constituent zeroth-order frozen waves and transverse SoP distributions of the resultant field at different propagation distances, respectively. The red and cyan ellipses in the bottom diagrams denote the local polarization ellipticity calculated from the measured Stokes parameters [11].

are  $|\mathbf{R}_0\rangle$  and  $|\mathbf{L}_0\rangle$ , respectively. In experiment, we set the initial phase difference,  $\varphi_0 = -\pi/2$ . Figure 3 shows the intensity patterns of two frozen waves as well as transverse SoP distributions of the resultant fields in equally spaced planes. The red and cyan ellipses in the bottom diagrams denote the local polarization ellipticity, which are calculated by measuring the Stokes parameters [11,26]. As expected, the resultant field changes its SoP along the red trajectory shown on a canonical Poincaré sphere upon propagation. These results indicate that the preshaped intensity profiles of frozen waves give rise to the longitudinal variation of the SoP.

Next, we engineer several polarization oscillating beams with inhomogeneously transverse SoPs. Figure 4(a) displays the measured intensity profiles of two first-order frozen waves possessing  $|\mathbf{R}_1\rangle$  and  $|\mathbf{L}_{-1}\rangle$  states with  $\varphi_0 = -\pi/2$  at a fixed point in the central ring in the transverse plane. The dots and curves correspond to the measured and analyzed results, respectively. It is well known, in the nondiffractive region, Bessel beams actually present Gauss-like intensity profiles [27], while these two first-order frozen waves present preshaped intensity profiles as sinusoidal curves. Clearly, the elaborated intensity profiles are complementary to each other, indicating

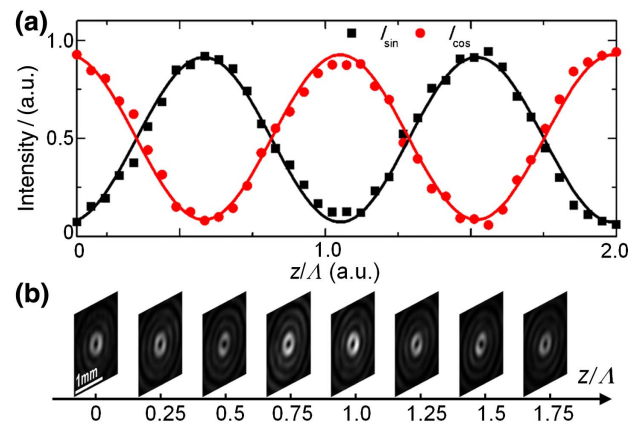


**Fig. 4.** (a) Longitudinal intensity distributions of two first-order frozen waves (denoted as red dots and black squares) with sinusoidal profiles. Dots, experiment result; curves, analyzed results. (b) Lateral intensity patterns of the synthesized field in equally spaced planes.

that the resultant field has a uniform intensity profile. Figure 4(b) sectionally displays transverse intensity distributions of the synthesized field in equally spaced planes. Obviously, the synthesized field presents a first-order Bessel functional intensity pattern. It should be noted that, experimentally, incomplete elimination of intensity that is inevitably induced by the extinction ratio of polarization analyzer debases the resultant quality.

To demonstrate the longitudinal variation of SoP, we measure the local SoP by utilizing the Stokes method [26]. Figure 5 displays the SoP and  $S_3$  distributions at different propagation distances. As shown in Fig. 4(b), the energy of the first-order Bessel beam almost concentrates in the central bright ring, which is the backbone of a Bessel beam. Hence, we just present the SoP distributions within the central region of Bessel beams. Besides, we note that, for a standing wave, a characteristic parameter is the node where the amplitude is minimal. Likewise, here we introduce node and antinode concepts to define the location where two frozen waves have minimal and maximum intensity differences. Obviously, the synthesized field has two important nodes and antinodes that correspond to typical SoP distributions. Here the nodes correspond to the diagonal and antidiagonal points on the equator of a higher-order Poincaré sphere, while the antinodes correspond to the poles where the synthesized field has homogeneous circular polarization. For such a special case, the SoPs of two nodes are denoted by  $|A_{1,-1}\rangle$  and  $|D_{1,-1}\rangle$  states, namely, the  $\pi$ -vector fields [21]. The characterized SoP distributions are shown in Figs. 5(a) and 5(b), respectively, where the black line and colored background depict the local SoP, i.e., polarization ellipticity  $\chi$  and orientation  $\psi$ , which are calculated according to the relationships  $\sin(2\chi) = S_3$  and  $\tan(2\psi) = S_2/S_1$ .

Figures 5(c)–5(f) orderly display the SoP (left column) and  $S_3$  (right column) distributions at two adjacent nodes and antinodes in an SoP conversion period. Remarkably, at

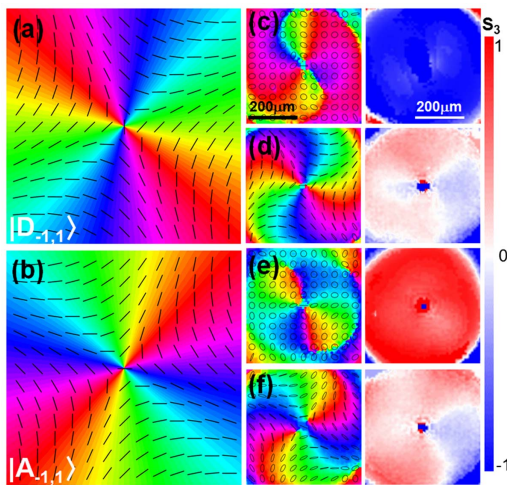


**Fig. 5.** (a), (b) SoP distributions of the  $|D_{-1,1}\rangle$  and  $|A_{-1,1}\rangle$  states. (c)–(f) Experimentally measured SoP distributions at two adjacent nodes and antinodes. Left, polarization orientation (background) and polarization ellipticity distributions; right,  $S_3$  distributions. Black line and ellipse depict the linear and ellipse polarizations, respectively.

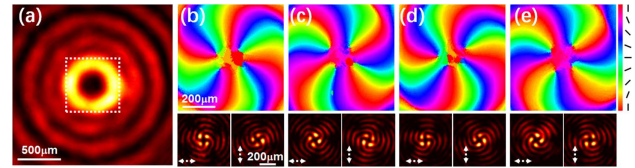


**Fig. 6.** (a) Intensity pattern of the second-order field at the  $z = 0$  plane. (b)–(e) Polarization orientation (upper) and intensity (bottom) distributions in four adjacent nodal planes. Arrows, the orientation of linear polarizer; dashed square, bound of selected areas corresponding to (b)–(e).

antinodes, the synthesized field alternately presents the homogeneous left- and right-handed circular polarizations, i.e.,  $S_3 = \pm 1$ , as shown in Figs. 5(c) and 5(e), while at nodes, it is transformed into  $\pi$ -vector SoPs with  $S_3 = 0$ , as shown in Figs. 5(d) and 5(f). As a whole, the transverse SoP structure also varies along the red trajectory, as shown in Fig. 1(c), but on a first-order Poincaré sphere.

We further construct a polarization oscillating beam with a second-order SoP, and the experimental results are shown in Fig. 6. Figure 6(a) shows the transverse intensity pattern at the  $z = 0$  plane, and Figs. 6(b)–6(e) display the polarization orientation and intensity patterns after a horizontal or vertical polarizer in four adjacent nodal planes, respectively. The dashed square depicts the boundary of Figs. 6(b)–6(e). The arrows denote the orientation of the linear polarizer. From these results, it can be seen that the synthesized field has the characteristics of a second-order vector Bessel beam, of which the polarization orientation rotates  $4\pi$  in a circle along the azimuthal direction. Moreover, these presentations demonstrate that the transverse SoP of the synthesized field oscillates periodically along the propagating direction.

In addition, we expand this method to the Bessel beam with a larger order. Figure 7(a) presents the resultant intensity distributions of a fifth-order polarization oscillating beam. Figures 7(b)–7(d) correspond to the intensity patterns of the vertical component in three adjacent nodal planes. Likewise, central ten-petal patterns demonstrate the successful generation of a fifth-order vector Bessel beam. The rotation of intensity pattern indicates the SoP conversion. Meanwhile, the identical patterns in Figs. 7(b) and 7(d) further demonstrate the periodic oscillation feature of the SoP.

As a whole, the above results demonstrate that the resultant field constructed from two copropagating frozen waves periodically oscillates its SoP along the propagating axis, maintaining a uniform intensity profile at a defined propagation distance. So, we name such a field as a polarization oscillating beam. It is

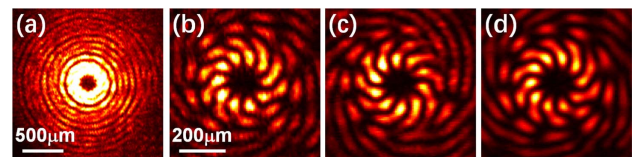


**Fig. 7.** (a) Intensity distribution of fifth-order field at the  $z = 0$  plane; (b)–(d) zoom-in vertical component distributions at three adjacent nodal planes.

apparent from the above analysis that our achievement approach can be extended to such attractive and efficient flatness optical elements as liquid crystal plates [28–30], metasurfaces [31–33], and subwavelength gratings [34–36]. In addition, the longitudinal SoP conversion process, that is, the transformation trajectory on all kinds of Poincaré spheres, is controllable by steering orthogonal basic states and initial phase differences [16]. Importantly, the preshaped feature of frozen waves in turn enriches the transformation speed of SoP, and other conversion such as nonlinear conversion is possible, giving rise to many intriguing byproducts such as inhomogeneous optical force [37] and spin-orbital coupling [38–40].

#### 4. CONCLUSION

In conclusion, we presented a class of polarization oscillating beams composed of two copropagating frozen waves with stationary fields and orthogonal SoPs. Four kinds of polarization oscillating beams with fundamental and higher-order SoPs were created to demonstrate the feasibility of our approach. These polarization oscillating beams with long periods have potential scientific and applied interests in optical manipulation, light guiding of atoms, polarization-sensitive sensing, and so on.

**Funding.** National Natural Science Foundation of China (NSFC) (11634010, 11774289, 61675168, 61377035); National Key Research and Development Program of China (2017YFA0303800); Fundamental Research Funds for the Central Universities (3102018zy036).

#### REFERENCES

- L. D. Barron, "Parity and optical activity," *Nature* **238**, 17–19 (1972).
- X. Fang, K. F. MacDonald, E. Plum, and N. I. Zheludev, "Coherent control of light-matter interactions in polarization standing waves," *Sci. Rep.* **6**, 31141 (2016).
- K. Y. Bliokh, Y. S. Kivshar, and F. Nori, "Magnetolectric effects in local light-matter interactions," *Phys. Rev. Lett.* **113**, 033601 (2014).
- E. Plum, K. F. MacDonald, X. Fang, D. Faccio, and N. I. Zheludev, "Controlling the optical response of 2D matter in standing waves," *ACS Photon.* **4**, 3000–3011 (2017).
- K. Y. Bliokh and F. Nori, "Transverse and longitudinal angular momenta of light," *Phys. Rep.* **592**, 1–38 (2015).
- P. W. Smorenburg, J. H. M. Kanters, A. Lassise, G. J. H. Brussaard, L. P. J. Kamp, and O. J. Luiten, "Polarization-dependent ponderomotive gradient force in a standing wave," *Phys. Rev. A* **83**, 063810 (2011).
- J. L. Everett, G. T. Campbell, Y.-W. Cho, P. Vernaz-Gris, D. B. Higginbottom, O. Pinel, N. P. Robins, P. K. Lam, and B. C. Buchler, "Dynamical observations of self-stabilizing stationary light," *Nat. Phys.* **13**, 68–73 (2016).
- N. Yang, Y. Tang, and A. E. Cohen, "Spectroscopy in sculpted field," *Nano Today* **4**, 269–279 (2009).
- Y. Tang and A. E. Cohen, "Enhanced enantioselectivity in excitation of chiral molecules by superchiral light," *Science* **332**, 333–336 (2011).
- L. Kang, Q. Ren, and D. H. Werner, "Leveraging superchiral light for manipulation of optical chirality in the near-field of plasmonic metamaterials," *ACS Photon.* **4**, 1298–1305 (2017).
- P. Li, Y. Zhang, S. Liu, L. Han, H. Cheng, and J. Zhao, "Quasi-Bessel beams with longitudinally varying polarization state generated by employing spectrum engineering," *Opt. Lett.* **41**, 4811–4814 (2016).
- F. Cardano, E. Karimi, L. Marrucci, C. de Lisio, and E. Santamato, "Generation and dynamics of optical beams with polarization singularities," *Opt. Express* **21**, 8815–8820 (2013).
- I. Moreno, J. A. Davis, M. M. Sánchez-López, K. Badham, and D. M. Cottrell, "Nondiffracting Bessel beams with polarization state that varies with propagation distance," *Opt. Lett.* **40**, 5451–5454 (2015).
- J. A. Davis, I. Moreno, K. Badham, M. M. Sánchez-López, and D. M. Cottrell, "Nondiffracting vector beams where the charge and the polarization state vary with propagation distance," *Opt. Lett.* **41**, 2270–2273 (2016).
- S. Fu, S. Zhang, and C. Gao, "Bessel beams with spatial oscillating polarization," *Sci. Rep.* **6**, 30765 (2016).
- P. Li, Y. Zhang, S. Liu, H. Cheng, L. Han, D. Wu, and J. Zhao, "Generation and self-healing of vector Bessel-Gauss beams with variant state of polarizations upon propagation," *Opt. Express* **25**, 5821–5831 (2017).
- M. Zamboni-Rached, "Stationary optical wave fields with arbitrary longitudinal shape by superposing equal frequency Bessel beams: frozen waves," *Opt. Express* **12**, 4001–4006 (2004).
- T. A. Vieira, M. R. R. Gesualdi, and M. Zamboni-Rached, "Frozen waves: experimental generation," *Opt. Lett.* **37**, 2034–2036 (2012).
- T. A. Vieira, M. R. R. Gesualdi, M. Zamboni-Rached, and E. Recami, "Production of dynamic frozen waves: controlling shape, location (and speed) of diffraction-resistant beams," *Opt. Lett.* **40**, 5834–5837 (2015).
- Z. Liu, Y. Liu, Y. Ke, Y. Liu, W. Shu, H. Luo, and S. Wen, "Generation of arbitrary vector vortex beams on hybrid-order Poincaré sphere," *Photon. Res.* **5**, 15–21 (2017).
- G. Milione, H. I. Sztul, D. A. Nolan, and R. R. Alfano, "Higher-order Poincaré sphere, Stokes parameters, and the angular momentum of light," *Phys. Rev. Lett.* **107**, 053601 (2011).
- X. Wang, J. Ding, W. Ni, C. Guo, and H. Wang, "Generation of arbitrary vector beams with a spatial light modulator and a common path interferometric arrangement," *Opt. Lett.* **32**, 3549–3551 (2007).
- X. Wang, Y. Li, J. Chen, C. Guo, J. Ding, and H. Wang, "A new type of vector fields with hybrid states of polarization," *Opt. Express* **18**, 10786–10795 (2010).
- X. Wang, J. Chen, Y. Li, J. Ding, C. Guo, and H. Wang, "Optical orbital angular momentum from the curl of polarization," *Phys. Rev. Lett.* **105**, 253602 (2010).
- J. Durnin, J. J. Miceli, Jr., and J. H. Eberly, "Diffraction-free beams," *Phys. Rev. Lett.* **58**, 1499–1501 (1987).
- P. Li, Y. Zhang, S. Liu, C. Ma, L. Han, H. Cheng, and J. Zhao, "Generation of perfect vectorial vortex beams," *Opt. Lett.* **41**, 2205–2208 (2016).
- T. Čižmár and K. Dholakia, "Tunable Bessel light modes: engineering the axial propagation," *Opt. Express* **17**, 15558–15570 (2009).
- P. Chen, S. Ge, W. Duan, B. Wei, G. Cui, W. Hu, and Y. Lu, "Digitalized geometric phases for parallel optical spin and orbital angular momentum encoding," *ACS Photon.* **4**, 1333–1338 (2017).
- L. Marrucci, C. Manzo, and D. Paparo, "Pancharatnam-Berry phase optical elements for wave front shaping in the visible domain: switchable helical mode generation," *Appl. Phys. Lett.* **88**, 221102 (2006).
- L. Marrucci, C. Manzo, and D. Paparo, "Optical spin-to-orbital angular momentum conversion in inhomogeneous anisotropic media," *Phys. Rev. Lett.* **96**, 163905 (2006).
- S. B. Glybovski, S. A. Tretyakov, P. A. Belov, Y. S. Kivshar, and C. R. Simovski, "Metasurface: from microwaves to visible," *Phys. Rep.* **634**, 1–72 (2016).
- L. Zhang, S. Mei, K. Huang, and C. Qiu, "Advances in full control of electromagnetic waves with metasurfaces," *Adv. Opt. Mater.* **4**, 818–833 (2016).
- N. Yu and F. Capasso, "Flat optics with designer metasurfaces," *Nat. Mater.* **13**, 139–150 (2014).
- W. Shu, X. Ling, X. Fu, Y. Liu, Y. Ke, and H. Luo, "Polarization evolution of vector beams generated by q-plates," *Photon. Res.* **5**, 64–72 (2017).
- Y. Ke, Y. Liu, J. Zhou, Y. Liu, H. Luo, and S. Wen, "Optical integration of Pancharatnam-Berry phase lens and dynamical phase lens," *Appl. Phys. Lett.* **108**, 101102 (2016).
- G. Biener, Y. Gorodetski, A. Niv, V. Kleiner, and E. Hasman, "Manipulation of polarization-dependent multivortices with quasi-periodic subwavelength structures," *Opt. Lett.* **31**, 1594–1596 (2006).

37. T. Zhang, M. R. C. Mahdy, Y. Liu, J. H. Teng, C. T. Lim, Z. Wang, and C. Qiu, "All-optical chirality-sensitive sorting via reversible lateral forces in interference fields," *ACS Nano* **11**, 4292–4300 (2017).
38. S. Liu, M. Wang, P. Li, P. Zhang, and J. Zhao, "Abrupt polarization transition of vector autofocusing Airy beams," *Opt. Lett.* **38**, 2416–2418 (2013).
39. S. Liu, P. Li, Y. Zhang, X. Gan, M. Wang, and J. Zhao, "Longitudinal spin separation of light and its performance in three-dimensionally controllable spin-dependent focal shift," *Sci. Rep.* **6**, 20774 (2016).
40. A. Aleksanyan and E. Brasselet, "Spin-orbit photonic interaction engineering of Bessel beams," *Optica* **3**, 167–174 (2016).